Comparative developmental transcriptomics of *Drosophila* mushroom body neurons highlights the mevalonate pathway as a regulator of axon growth

Lora Fahdan[1,2], Hagar Meltzer[1,2], Noa Wigoda[3], Ron Rotkopf[3], Oren Schuldiner [1,2*]

[1] Department of Molecular Cell Biology, Weizmann Institute of Science, Rehovot, Israel
[2] Department of Molecular Neuroscience, Weizmann Institute of Science, Rehovot, Israel
[3] Bioinformatics unit, Department of Life Sciences Core Facilities, Weizmann Institute of Science, Rehovot, Israel

[*] Correspondence to: oren.schuldiner@weizmann.ac.il

Abstract

The ability of neurons to extend axons is governed by tightly regulated genetic programs that vary across developmental stages and cell types. Understanding the molecular features that control axon growth potential is critical for uncovering how neural circuits form, mature, and respond to injury or disease. The *Drosophila* mushroom body (MB) offers a powerful model to dissect axon growth programs, as lineage-related Kenyon cells (KCs) undergo different developmental events under shared spatiotemporal conditions. During metamorphosis, γ-KCs undergo axon pruning, followed by developmental regrowth at the same time-frame as α/β-KCs initiate axon growth - thus providing a unique opportunity to compare these distinct growth paradigms. We thus performed RNA-sequencing of α/β- and γ-KCs during their initial growth and developmental regrowth, respectively, revealing dynamic transcriptional changes and identifying 300 shared genes upregulated during both growth states. A targeted loss-of-function screen revealed genes specifically required for either α/β initial growth, γ regrowth, or both. Focusing on one such candidate, Pmvk, we found that it plays a crucial role in axon regrowth by acting within the mevalonate pathway. Notably, other enzymes in this pathway were also required, suggesting that the entire metabolic pathway is essential for supporting regrowth. Genetic mutant analyses and rescue exepriements suggest that Pmvk likely controls axon regrowth via Rheb, an effector of the TOR pathway, which we previously found to be required for regrowth. Our developmental transcriptomic atlas not only advances understanding of intrinsic axon growth programs, but also provides candidate genes and a valuable framework for future studies aimed at enhancing axon regeneration in the adult nervous system.

Introduction

Axon growth is essential for correct circuit formation during development. It is a tightly controlled process, and an emerging paradigm claims that axon growth and synaptogenesis are mutually exclusive processe (Bradke, 2022; Hilton et al., 2022). Despite its significance, the cellular and molecular mechanisms that govern different axon growth states are not fully understood. Axon growth capacity is also crucial during regeneration following injury. Santiago Ramon y Cajal (Rozo et al., 2024) first noted that while the adult mammalian central nervous system typically fails to regenerate, the peripheral nervous system can sprout and grow new connections. Regeneration is influenced by both intrinsic factors that determine axon growth potential, and extrinsic factors such as deposits by glia or other cells (Sutherland and Geoffroy, 2020; Zheng and Tuszynski, 2023). Therefore, understanding how intrinsic axon growth capacity is mechanistically regulated in different developmental contexts should also forward our understanding of what limits axon regeneration in pathological states such as spinal cord injury.

Drosophila is an excellent model organism to investigate axon growth potential in different developmental contexts, due to its unparalleled neurogenetic toolkit combined with the extensive remodeling of its nervous system during metamorphosis. Neuronal remodeling is a conserved strategy to refine neural circuits, by eliminating exuberant connections and promoting regrowth toward adult-specific targets (Schuldiner and Yaron, 2015). The *Drosophila* mushroom body (MB), a center of associative learning and memory in the fly brain (Belle and Heisenberg, 1994), undergoes stereotypic remodeling during early pupal stages. The MB is comprised of three major types of intrinsic neurons: the γ-, α′/β′- and α/β-Kenyon Cells (KCs), sequentially born from four neuroblasts per hemisphere (Lee et al., 1999). The first-born γ-KCs initially extend axons that bifurcate to form the larval vertical and medial lobes. However, in early pupae (initiated at ~6 hours after puparium formation; h APF), both axonal lobes are pruned back to their branch point, followed by axon regrowth (initiated at ~24h APF) to form the adult-specific γ lobe that only projects medially (Lee et al., 1999). In contrast, the later-born α′/β′- and α/β-KCs retain their original bifurcated projections into adulthood (Figure 1A). Importantly, the initial growth of

α/β-axons occurs at ~24h APF – the same time in which γ-axons initiate developmental regrowth.

γ-axons thus undergo dynamic transitions between intial growth, pruning, and regrowth, all of which were shown to be tightly regulated by nuclear receptor complexes (Lee et al., 2000; Rabinovich et al., 2016; Yaniv et al., 2012), implying they are goverened by genetic programs. We previously employed RNA-sequencing to characterize the transcriptional landscape of γ-KCs throughout development at high temporal resolution (Alyagor et al., 2018). Moreover, our lab demonstrated that the molecular mechanisms underyling developmental regrowth are distinct from those of initial axon growth, yet show similarities to regeneration after injury (Marmor-Kollet and Schuldiner, 2016; Rabinovich et al., 2016; Sudarsanam et al., 2020; Yaniv et al., 2020). The fact that different axon growth states share core machinery yet also show distinct pathways depending on the cellular and developmental context, motivated us to directly compare the genetic programs of initial axon growth and developmental axon regrowth.

In this study, we took advantage of the temporal overlap between α/β initial growth and γ regrowth to compare the transciptional landscape of these distinct axon growth programs occuring in a similar developmental, environmental and lineage context (Figure 1A-B). This comparison laid the groundwork for a large-scale loss-of-function screen aimed at uncovering genes and pathways required for both axon growth paradigms. Through this approach, we identified 12 genes that are required for initial axon growth and/or regrowth. We delved deeper into phosphomevalonate kinase (Pmvk), an enzyme in the mevalonate pathway, and found that it likely promotes axon regrowth, but not initial growth, at least in part via the TOR pathway. Together, our findings reveal shared and divergent molecular pathways underlying distinct axon growth programs, offering new insights into how intrinsic factors shape neuronal growth capacity. By combining time-course transcriptional profiling of defined neuronal populations with functional genetics, we not only uncovered key regulators of axon regrowth, but also provide a rich, publicly available dataset that can serve as a foundation for future discoveries in neuronal development.

139 **Methods**

140 **Key resources table**

Reagent or resource	Source	Identifier
Antibodies		
Chicken anti GFP 1:500	AVES	Cat#GFP-1020; RRID: AB_10000240
Mouse monoclonal anti FasII 1:25	Developmental Studies Hybridoma Bank (DSHB)	Cat#1D4; RRID:AB_528235
Mouse monoclonal anti dac 1:10	Developmental Studies Hybridoma Bank (DSHB)	Cat#mAbdac2-3;RRID: AB_528190
Goat anti mouse Alexa fluor 647 1:300	Invitrogen	Cat#A32728; RRID:AB_2633277
FITC goat anti chicken 1:300	Invitrogen	Cat#16055;RRID: AB_2534728
Chemicals, peptides, and recombinant proteins		
Cell dissociation solution	Sigma Aldrich	Cat# C1544
Collagenase/dispase mix	Roche	Cat# 10269638001
Critical commercial assays		
Pico pure RNA isolation kit	Life Technologies	Cat# KIT0204
Deposited Data		
Raw data files for developmental seq	NCBI Gene Expression Omnibus	GEO: GSE308165
Experimental models: organisms/strains		
w[1118];P{y[+t7.7]w[+mC]=GMR16B01GA4}attP2	BDSC	48712

w[1118];P{y[+t7.7]w[+mC]=GMR71G10GA4}attP2	BDSC	39604
w[*];P{y[+t7.7]w[+mC]=10XUASIVSmCD8::GFP}attP2	BDSC	32185
y[1]w[1118];P{w[+mC]=QUASmtdTomato3xHA}14/CyO	BDSC	30004
GMR71G10-QF2 (2nd Chromosome)	(Bornstein et al., 2015)	N/A
y[1]sc[*]v[1]sev[21];P{y[+t7.7]v[+t1.8]=TRiP.HMS00991}attP2 (UAS-emb RNAi)	BDSC	34021
y[1]sc[*]v[1]sev[21];P{y[+t7.7]v[+t1.8]=TRiP.HMS00347}attP2 (UAS-mira RNAi)	BDSC	32356
y[1]sc[*]v[1]sev[21];P{y[+t7.7]v[+t1.8]=TRiP.HMS00487}attP2 (UAS-chm RNAi)	BDSC	32484
y[1]sc[*]v[1]sev[21];P{y[+t7.7]v[+t1.8]=TRiP.HMC03533}attP2 (UAS-beag RNAi)	BDSC	53306
y[1]sc[*]v[1]sev[21];P{y[+t7.7]v[+t1.8]=TRiP.HMS01281}attP2 (UAS-CCT7 RNAi)	BDSC	34931
y[1]sc[*]v[1]sev[21];P{y[+t7.7]v[+t1.8]=TRiP.HMS05732}attP40 (UAS-twr RNAi)	BDSC	67881
y[1]sc[*]v[1]sev[21];P{y[+t7.7]v[+t1.8]=TRiP.HMS02380}attP2 (UAS-CadN RNAi)	BDSC	41982
y[1]v[1];P{y[+t7.7]v[+t1.8]=TRiP.HMS00909}attP2 (UAS-Bap60 RNAi)	BDSC	33954
y[1]v[1];P{y[+t7.7]v[+t1.8]=TRiP.GL01246}attP2 (UAS-CCT5 RNAi)	BDSC	41818
y[1]v[1];P{y[+t7.7]v[+t1.8]=TRiP.HMJ21725}attP40 (UAS-Hsp67Ba RNAi)	BDSC	53007
y[1]v[1];P{y[+t7.7]v[+t1.8]=TRiP.HMJ21488}attP40 (UAS-Dip-B RNAi)	BDSC	54045
y[1]v[1];P{y[+t7.7]v[+t1.8]=TRiP.HMJ21057}attP40/CyO (UAS-Pmvk RNAi)	BDSC	50955
P{hsFLP}1y[1]w[1118];P{HD_CFD00252}attP40/CyO-GFP (Pmvk gRNA)	VDRC	341218
Pmvk E20*/Cyo	This study	N/A
y[1]v[1];P{y[+t7.7]v[+t1.8]=TRiP.HMJ22759}attP40 (UAS-Mvk RNAi)	BDSC	60442
P{KK101807}VIE-260B (UAS-Hmgcr RNAi)	VDRC	108617
P{w[+mC]=UAS-Dcr-2.D}1	BDSC	24648

P{KK105673}VIE-260B (UAS-GGT1 RNAi)	VDRC	110288
y[1]v[1];P{y[+t7.7]v[+t1.8]=TRiP.HMJ21755}attP40 (UAS-Fntb RNAi)	BDSC	53029
y[1]sc[*]v[1]sev[21];P{y[+t7.7]v[+t1.8]=TRiP.GL01026}attP2 (UAS-FntaRNAi)	BDSC	36873
y[1]v[1];P{y[+t7.7]v[+t1.8]=TRiP.HMC03386}attP40 (UAS-Dhdds RNAi)	BDSC	51815
y[1]v[1];P{y[+t7.7]v[+t1.8]=TRiP.HMC03486}attP40 (UAS-Pdss2 RNAi)	BDSC	51910
w[1118]P{GD4696}v47001 (UAS-qm RNAi)	VDRC	47001
w[1118];P{w[+mC]=UAS-S6k.STDETE}2 (UAS-S6K^{CA})	BDSC	6914
w[*];P{w[+mC]=UAS-Rheb.Pa}3 (UAS-Rheb)	BDSC	9689
w[*];P{w[+mC]=UAS-Rho1.V14}2.1/TM6 (UAS-Rho)	BDSC	8144
y[1]v[1];P{y[+t7.7]v[+t1.8]=UASLUC.VALIUM10}attP2 (UAS- Luciferase)	BDSC	35788
Primers used for Pmvk mutation screening:	This study	N/A
TAAACACAACAGGCCGCAGT		
AATAGAGCTTGTGTGGCGGT		
Software and algorithms		
DEseq2	Love et al. (2014)	N/A
STAR	(Dobin et al., 2013)	N/A
FIJI	Image J	https://imagej.net/Fiji/Downloads
Other		
NovaSeq6000 instrument (Illumina)	Illumina	N/A
BD FACSAriaIII	BD Bioscience	N/A
Zeiss LSM 800 and 980 confocal microscope	Zeiss	N/A

141

142 **Fly husbandry and strains**

143 All fly strains were reared at 25°C (unless indicated otherwise) under standard laboratory
144 conditions on molasses-containing food. Unless specifically written, similar numbers of
145 male and female flies were taken. ‘Adult’ refers to flies 3-5 days post eclosion.

146 The 30 driver lines screened to specifically label α/β-KCs are described in Supplementary
147 Table 1. The RNAi lines used in the loss-of-function screen are detailed in Supplementry
148 Table 3.
149 RNAi lines were obtained from the Vienna Drosophila Resource Center (VDRC), Austria,
150 or from Bloomington Drosophila Stock Center (BDSC), USA.
151 **Genotypes**
152 hsFLP is y,w,hsFLP122; 40A and 82B are FRTs on 2L and 3R respectively; 71G10 is
153 GMR71G10-GAL4; 71G10-QF2 is GMR71G10-QF2; OK107 is OK107-GAL4; R44E04 is
154 GMR44E04-GAL4; 16B01 is GMR16B01-Gal4; G80 is TubP-Gal80. QUAS-mtdT is
155 QUAS-mtdt:HA, UAS-CD8:GFP is UAS-mCD8::GFP.
156 Males and females were used interchangeably.
157 Figure1:
158 (C) UAS-CD8:GFP/+;71G10/+
159 (D) UAS-CD8:GFP/+;16B01/+
160 Figure3:
161 (B) 71G10-QF2,QUAS-mtdT/+;UAS-Luciferase/+;OK107/+
162 (D) 71G10-QF2,QUAS-mtdT/+;UAS-beag RNAi$^{TRiP.HMC03533}$/+;OK107/+
163 (E) 71G10-QF2,QUAS-mtdT/+;UAS-chm RNAi$^{TRiP.HMS00487}$/+;OK107/+
164 (F) 71G10-QF2,QUAS-mtdT/+;UAS-Hsp67Ba RNAi$^{TRiP.HMJ21725}$/+;OK107/+
165 (H) 71G10-QF2,QUAS-mtdT/+;UAS-CCT5 RNAi^{HMC02988}/+;OK107/+
166 (I) 71G10-QF2,QUAS-mtdT/+;UAS-CCT7 RNAi$^{TRiP.HMS01281}$/+;OK107/+
167 (J) 71G10-QF2,QUAS-mtdT/+;UAS-emb RNAi$^{TRiP.GL01246}$/+;OK107/+
168 (K) 71G10-QF2,QUAS-mtdT/+;UAS-Dip-B RNAi$^{TRiP.HMJ21488}$/+;OK107/+
169 (L) 71G10-QF2,QUAS-mtdT/+;UAS-Bap60 RNAi$^{TRiP.HMS00909}$/+;OK107/+
170 (M) 71G10-QF2,QUAS-mtdT/+;UAS-Pmvk RNAi$^{TRiP.HMJ21057}$/+;OK107/+
171 (N) 71G10-QF2,QUAS-mtdT/+;UAS-twr RNAi$^{TRiP.HMS05732}$/+;OK107/+
172 (O) 71G10-QF2,QUAS-mtdT/+;UAS-cadN RNAi$^{TRiP.HMS02380}$/+;OK107/+
173 (Q) 71G10-QF2,QUAS-mtdT/+;UAS-mira RNAi$^{TRiP.HMS00347}$/+;OK107/+
174 Figure 4:
175 (A,C) 71G10,UAS-CD8:GFP/+;UAS-Luciferase/+
176 (B,D) 71G10,UAS-CD8:GFP/+;UAS- Pmvk RNAi $^{TRiP.HMJ21057}$/+

177 (E) R44E04,UAS-CD8:GFP/+;UAS-Luciferase/+

178 (F) R44E04,UAS-CD8:GFP/+;UAS- Pmvk RNAi $^{TRiP.HMJ21057}$/+

179 (G,I) hsFLP,UAS-CD8::GFP/+;G80,40A/40A;71G10/+

180 (H,J)hsFLP,CD8:GFP/+;UAS-PmvkRNAi $^{TRiP.HMJ21057}$(attP40)/+;82B,Gal80/82B;OK107/+

181 (K) hsFLP,UAS-CD8::GFP/+;G80,40A/40A;R44E04/+

182 (L) hsFLP,UAS-CD8::GFP/+;G80,40A/*Pmvk*^{E20*},40A;R44E04/+

183 Figure 5:

184 (A) 71G10-QF2,QUAS-mtdT/+;UAS-Luciferase/+;OK107/+

185 (B) UAS-Dicer;71G10-QF2,QUAS-mtdT/+;UAS-Hmgcr RNAi KK 101807/+;OK107/+

186 (C) 71G10-QF2,QUAS-mtdT/+;UAS-Mvk RNAi $^{TRiP.HMJ22759}$/+;OK107/+

187 Figure 6:

188 (C) hsFLP,UAS-CD8::GFP/+;G80,40A/40A;71G10/+

189 (D) hsFLP,UAS-CD8::GFP/+;G80,40A/*Pmvk*^{E20*},40A;71G10/+

190 (E) hsFLP,UAS-CD8::GFP/+;G80,40A/*Pmvk*^{E20*},40A;71G10/UAS-Rho

191 (F) hsFLP,UAS-CD8::GFP/+;G80,40A/*Pmvk*^{E20*},40A;71G10/UAS-Rheb

192 (G) hsFLP,UAS-CD8::GFP/+;G80,40A/*Pmvk*^{E20*},40A;71G10/UAS-S6K^{CA}

193 Figures S3:

194 (A) hsFLP,UAS-CD8:GFP;G80,40A/40A;OK107/+

195 (B) hsFLP,UAS-CD8:GFP;G80,40A/40A;UAS-emb RNAi$^{TRiP.HMS00991}$/+;OK107/+

196 (C) hsFLP,UAS-CD8:GFP;G80,40A/40A;UAS-CCT5 RNAi$^{TRiP.GL01246}$/+;OK107/+

197 (D) hsFLP,UAS-CD8:GFP;G80,40A/40A;UAS-CCT7 RNAi$^{TRiP.HMS01281}$/+;OK107/+

198 (E) hsFLP,UAS-CD8:GFP;G80,40A/40A;UAS-CadN RNAi$^{TRiP.HMS02380}$/+;OK107/+

199 (F) hsFLP,CD8:GFP/+;UAS-Pmvk RNAi $^{TRiP.HMJ21057}$/+;82B,G80/82B;OK107/+

200 (G) hsFLP,CD8:GFP/+;UAS-twr RNAi$^{TRiP.HMS05732}$/+;82B,G80/82B;OK107/+

201 (H) hsFLP,UAS-CD8:GFP;G80,40A/40A;UAS-Bap60 RNAi$^{TRiP.HMS00909}$/+;OK107/+

202 (I) hsFLP,CD8:GFP/+;UAS-Dip-B RNAi$^{TRiP.HMJ21488}$ /+;82B,G80/82B;OK107/+

203 (J) hsFLP,UAS-CD8:GFP;G80,40A/40A;UAS-beag RNAi$^{TRiP.HMC03533}$/+;OK107/+

204 (K) hsFLP,UAS-CD8:GFP;G80,40A/40A;UAS-chm RNAi$^{TRiP.HMS00487}$/+;OK107/+

205 (L) hsFLP,CD8:GFP/+;UAS-Hsp67Ba RNAi$^{TRiP.HMJ21725}$ /+;82B,G80/82B;OK107/+

206 (M) hsFLP,UAS-CD8:GFP;G80,40A/40A;UAS-mira RNAi$^{TRiP.HMS00347}$/+;OK107/+

207 Figures S4:

208 (A) hsFLP,UAS-CD8:GFP;G80,40A/40A;OK107/+
209 (B) hsFLP,UAS-CD8:GFP;G80,40A/40A;UAS-emb RNAi$^{TRiP.HMS00991}$/+;OK107/+
210 (C) hsFLP,UAS-CD8:GFP;G80,40A/40A;UAS-CCT5 RNAi$^{TRiP.GL01246}$/+;OK107/+
211 (D) hsFLP,UAS-CD8:GFP;G80,40A/40A;UAS-CCT7 RNAi$^{TRiP.HMS01281}$/+;OK107/+
212 Figure S5:
213 (B) 71G10-QF2, QUAS-mtdT/+;UAS-Luciferase/+;OK107/+
214 (C) UAS-Dicer;71G10-QF2,QUAS-mtdT/+;UAS-GGT1 RNAi KK 105673/+;OK107/+
215 (D)71G10-QF2,QUAS-mtdT/+;UAS-Fntb RNAi $^{TRiP.HMJ21755}$/+;OK107/+
216 (E) 71G10-QF2,QUAS-mtdT/+;UAS-Fnta RNAi $^{TRiP.GL01026}$/+;OK107/+
217 (F) 71G10-QF2,QUAS-mtdT/+;UAS-Dhdds RNAi $^{TRiP.HMC03386}$/+;OK107/+
218 (G) 71G10-QF2,QUAS-mtdT/+;UAS-Pdss2 RNAi $^{TRiP.HMC03486}$/+;OK107/+
219 (H) 71G10-QF2,QUAS-mtdT/+;UAS-qm RNAi GD 4696/+;OK107/+
220 Figure S6:
221 (A) hsFLP,UAS-CD8::GFP/+;G80,40A/40A;71G10/+
222 (B) hsFLP,UAS-CD8::GFP/+;G80,40A/40A;71G10/UAS-Rheb
223 (C) hsFLP,UAS-CD8::GFP/+;G80,40A/40A;71G10/UAS-Rho
224 (D) hsFLP,UAS-CD8::GFP/+;G80,40A/40A;71G10/UAS-S6K^{CA}
225 Figure S7:
226 (A) hsFLP,UAS-CD8::GFP/+;G80,40A/40A;71G10/+
227 (B) hsFLP,UAS-CD8::GFP/+;G80,40A/*Pmvk*^{E20*},40A;71G10/+
228 (C) hsFLP,UAS-CD8::GFP/+;G80,40A/*Pmvk*^{E20*},40A;71G10/UAS-Rho
229 (D) hsFLP,UAS-CD8::GFP/+;G80,40A/*Pmvk*^{E20*},40A;71G10/UAS-Rheb
230 (E) hsFLP,UAS-CD8::GFP/+;G80,40A/*Pmvk*^{E20*},40A;71G10/UAS-S6K^{CA}
231 **Materials and methods**
232 **Cell dissociation and sorting**
233 Brains were dissected in a cold Ringer's solution and incubated at 29°C with a
234 collagenase/dispase mix for 15 minutes for larval and pupal brains, and 30 minutes for
235 adult brains. After enzymatic digestion, the tissue was washed with a dissociation solution
236 (Sigma-Aldrich) and mechanically dissociated into single cells. The cell suspension was
237 then passed through a 35µm mesh (Falcon) to remove debris and cell clusters. A total of
238 1000 GFP+ cells were sorted using a BD FACSAriaIII (BD Biosciences) equipped with a

239 100μm nozzle under low pressure, directly into 100μl of Pico-Pure RNA isolation kit
240 extraction buffer (Life Technologies). RNA extraction was subsequently performed using
241 the kit, or frozen at -80°C for future use. To minimize potential injury responses, samples
242 were kept on ice throughout the procedure, from dissection to RNA extraction except from
243 the dissociation enzyme incubation.

244 **RNA amplification and library preparation**

245 **Bulk smart-seq2**

246 Bulk RNA-seq libraries were prepared at the Crown Genomics Institute of the Nancy and
247 Stephen Grand Israel National Center for Personalized Medicine (G-INCPM), Weizmann
248 Institute of Science. Libraries were prepared based on the smart-seq2 protocol (Picelli et
249 al., 2014) with small modifications. Briefly, 250 pg of RNA was used as input. Reverse
250 transcription was performed using Oligo-dT primers, followed by PCR (16 cycles). After
251 Agencourt Ampure XP beads cleanup (Beckman Coulter), the amplified cDNA underwent
252 library generation using Nextera XT (Illumina). Libraries were quantified by Qubit (Thermo
253 Fisher Scientific) and TapeStation (Agilent). Sequencing was done on a NovaSeq6000
254 instrument (Illumina) using an SP 100 cycles kit, allocating approximately 13M reads per
255 sample (single read sequencing).

256 **Analysis of RNA-Seq data**

257 Two sequencing runs of RNA were combined, yielding a mean of 22.5 million reads
258 (single-read sequencing) and a minimum of 10 million reads per sample. The reads were
259 aligned with STAR **(DOI: 10.1093/bioinformatics/bts635)** v2.5.2 to the reference
260 genome of *Drosophila melanogaster* (DM6, UCSC). Gene annotations were obtained
261 from FlyBase.org (Dmel r6.46). Gene expression levels were quantified using STAR.
262 12,493 genes had been identified in total across the two datasets (in either γ or α/β or
263 both). Out of these, only genes that were expressed in at least four samples (replicates)
264 of a single time point (condition) were kept, so that the 8,221 genes that met this
265 requirement were used in further analysis. To get relevant p-values and fold-changes for
266 comparisons of a condition with all-zeros vs. a condition with non-zero value, zero values
267 were replaced with randomly assigned numbers between 1 and 7. The updated count
268 matrix was subjected to normalization and statistical analysis using the UTAP2 pipeline
269 (Lindner et al., 2025) which took batch effects into account and employed the DESeq2

algorithm (Love et al., 2014). Genes were considered differentially expressed if they had an adjusted p-value (padj) ≤ 0.05, a fold change ≥ 1.5 and a mean read counts of ≥10 reads.

Clusters and sub-clusters generation and analysis

Based on the α/β transcriptome, gene expression at each of the five developmental stages (18, 21, 24, 27, and 30 hours APF) was compared to the adult stage. Genes were classified as differentially expressed during development if, at any time point, their expression was at least 1.5-fold different from the adult expression, with an adjusted p-value (padj) < 0.05 and a mean read count of at least 10, resulting in the identification of 3,345 genes. Using Partek™ Genomics Suite (version 7), we performed k-means clustering on the mean expression across replicates at each developmental time point, selecting k = 8 after testing multiple values, as this produced the most distinct and coherent clusters. For subclustering the α/β Cluster 1 and Cluster 2, we employed k-means clustering based on the average expression of those genes in γ-KCs across replicates at each time point. Cluster 1 was further subdevided into 10 additional subclusters 1A-J, and cluster 2 into 7 subclusters 2A-G. We identified statistically enriched terms using Metascape (Zhou et al., 2019). This tool integrates multiple authoritative databases to identify enriched Gene Ontology (GO) terms, canonical pathways, and functional gene groups. For each cluster, the input gene lists were analyzed against the default background, and significantly enriched categories were reported based on a hypergeometric test with multiple-testing correction. The resulting enrichment networks and bar plots were used to interpret the biological processes and pathways associated with each gene cluster.

Immunohistochemistry

Brains were dissected in cold Ringer's solution, fixed with 4% paraformaldehyde (PFA) for 20 minutes at room temperature (RT), and subsequently washed in phosphate buffer (PB) containing 0.3% Triton-X (PBT). The washing protocol consisted of three rapid rinses followed by three additional washes, each lasting 20 minutes. To minimize non-specific staining, the samples were incubated in PBT supplemented with 5% heat-inactivated goat serum. They were then treated with primary antibodies overnight at 4°C, followed PBT washes (as above), then incubation with secondary antibodies for 2 hours at RT, followed

301 by PBT washes. The brains were then mounted using SlowFade (Invitrogen) and
302 visualized using Zeiss LSM800 or LSM980 confocal microscopes. Image analysis was
303 carried out with ImageJ 1.51 (NIH).

304 **Generation of CRISPR mutant flies**

305 To generate the Pmvk mutant, we used a fly strain (VDRC#341218) that expresses two
306 guide RNAs (sgRNAs) under the control of a UAS promoter. These sgRNAs target coding
307 exons in the 5′ region of the Pmvk gene, without overlapping the start codon. This design
308 facilitates the introduction of small insertions or deletions (indels) in the presence of Cas9.
309 To drive germline mutagenesis, we incorporated a nanos-Gal4 on the third chromosome
310 and crossed these flies with a UAS-Cas9 expressing fly, which also carries a 40A FRT
311 site on the second chromosome. After two generations, individual males were crossed
312 with balancer flies for mutation screening. We recovered a Pmvk mutant allele that
313 contained a nucleotide substitution (G>T) at position 60 ($Pmvk^{E20*}$, Figure 4G).

314 **MARCM analysis**

315 Mosaic Analysis with a Repressible Cell Marker (MARCM) clones were generated in a
316 similar strategy as previously described (Lee and Luo, 1999). To generate γ- or α/β-
317 clones, newly hatched larvae (NHL) or pupae at 0h APF, respectively, underwent a heat
318 shock treatment at 37°C for 40 minutes. Larvae and pupae were then transferred to a
319 25°C incubator where they remained until eclosion.

320 **Data and software availability**

321 The data discussed in this publication have been deposited in NCBI's Gene Expression
322 Omnibus and are accessible through GEO series accession number GEO: GSE308165
323 (https://www.ncbi.nlm.nih.gov/geo/query/acc.cgi?acc=GSE308165)

324 **Regrowth quantification**

325 To quantify regrowth, we used a method described in a previous publication (Bornstein
326 et al., 2021) and illustrated in Figure 6. Two reference lines were extended: line y (red),
327 representing the full length of the γ-lobe (determined based on FasII staining), and line x
328 (yellow), indicating the extent of clonal γ-axon regrowth (determined as the most distal
329 point the axons reach). The regrowth index was calculated as the ratio of x to y (x/y),
330 providing a normalized measure of axonal regrowth.

Statistical analyses for regrowth quantification were performed in R, v.4.5.1. Proportional data were logit-transformed prior to testing to meet assumptions of normality and homogeneity of variance. Group differences were evaluated using one-way ANOVA, followed by Dunnett's post hoc test comparing all groups to Pmvk. A significant difference was detected only between control and *Pmvk*^{E20*} ($p < 0.001$).

362 **Results**

363 **Lineage-related neuronal types in the *Drosophila* mushroom body undergo intial**
364 **axon growth and developmental regrowth in similar spatiotemporal conditions**

365 In a previous study (Alyagor et al., 2018), we found that the developmental age was by
366 far the most dominant factor in defining the transcriptional profile of γ-KCs - a principle
367 that was later observed in developing projection neurons as well (Xie et al., 2021).
368 Remarkably, adult γ-KCs were more similar, on a global level, to other adult neurons than
369 to larval or pupal γ-KCs. Notably, while initial axon growth occurs in embyonic and early
370 larval life, developmental regrowth occurs during metamorphosis. Therefore, to reliably
371 compare the genetic programs of initial axon growth and developmental regrowth, we
372 sought to profile two similar neuronal types that undergo different axon growth states at
373 the same developmental window. The lineage-related α/β- and γ-KCs were a perfect
374 match, as within a similar timeframe during the pupal stage, α/β-KCs extend their axons
375 for the first time, while γ-KCs regrow their axons after pruning (Figure 1A-B).

376 To achieve our goal, we screened for drivers that would specifically label α/β-KCs at the
377 pupal stage, when they send out axonal processes. We screened 30 Gal4 driver lines
378 considered to be α/β-specific in adult flies (Supplementary Table 1), and imaged them at
379 24h APF. To our surprise, only one line - R16B01-Gal4 - was specific to the MB (i.e., not
380 expressed elsewhere in the brain), and within the MB, specific to α/β-KCs throughout their
381 growth (Figure 1C). At 18h APF, α/β-KCs labeled with R16B01-Gal4 showed cell bodies
382 with short, loosely arranged axons that were still difficult to follow. By 21h APF, these
383 axons had gathered into a tight bundle, and their growing axon tips were visible.
384 Observations throughout the pupal stage revealed that these axons extended and
385 reached the tips of the lobes by 36h APF (Figure 1C).

386 Identifying this driver enabled us to isolate α/β-KCs throughout their initial axon growth.
387 For comparative purposes, we also repeated the isolation and profiling of γ-KCs, as
388 previously done in our lab (Alyagor et al., 2018), using the same driver that specifically
389 labels developing γ-KCs (R71G10-Gal4; Figure 1D). Labeling both types of neurons gave
390 us the opportunity to isolate and sequence each population while they extend their axons
391 for the first (α/β) or second (γ) time. Altogether, we sorted and sequenced α/β- and γ-KCs
392 at 5 pupal timepoints - every three hours from 18h until 30h APF - in addition to adult.

We used Principal Component Analysis (PCA) to compare the transcriptional profiles of developing and adult α/β- and γ-KCs. Our results confirmed our prior knowledge (Alyagor et al., 2018) that adult γ- or α/β-KCs are more similar to each other than to their own developmental forms. Notably, developing γ- and α/β-KCs occupied a specific region in the PCA space (Figure 1E).

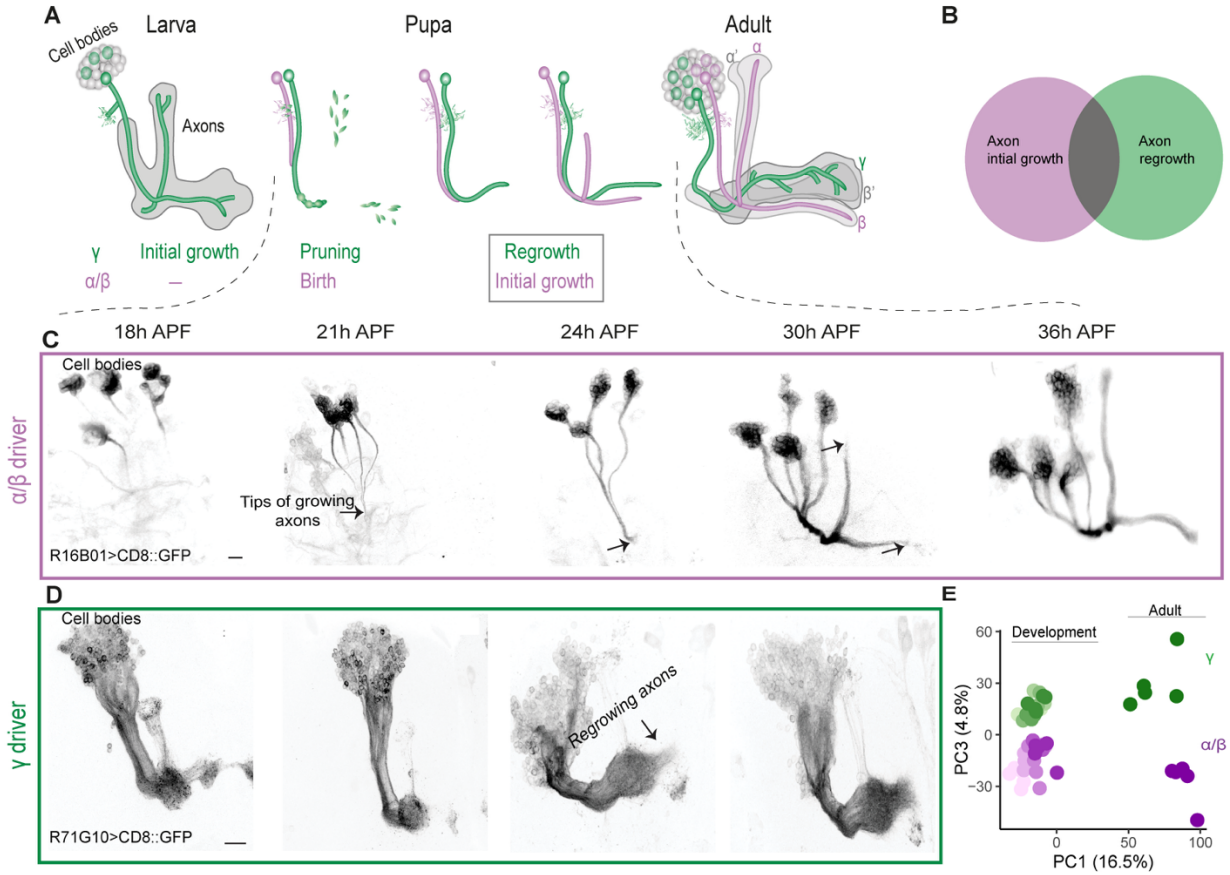

Figure 1. Lineage-related neuronal types undergo intial axon growth and regrowth in shared spatiotemporal conditions. (A) A model of MB development highlighting that the regrowth of γ-axons temporally and spatially overlaps with the initial growth of α/β-axons.

(B) A Venn diagram depicting the theoretical and predicted comparison between α/β initial axon growth and γ-axon regrowth.

(C) Confocal Z-projections of R16B01-Gal4 driving expression of membranal GFP (mCD8::GFP), which specifically labels developing α/β-KCs during the pupal stage. The images were captured at five time points between 18h until 36h APF, when the axons reach the end of the lobes. At 18h APF, four groups of cell bodies can be observed, corresponding to newly born cells from the four neuroblasts, each sending out short axons that progressively extend in each subsequent image. The axon tips are marked with arrows.

412 (D) Confocal Z-projections of γ-KCs labeled with R71G10-Gal4 driving mCD8::GFP, as
413 identified by (Alyagor et al., 2018), between 18h to 30h APF. At 21h APF, the axons are
414 completely pruned and begin to re-extend for a second time. By 24h APF, the regrowing
415 axons are visible (arrow).
416 (E) PCA of α/β and γ-KC expression profiles during development and in adult. Color code
417 depicts neuronal type (green for γ and magenta for α/β) and developmental stage (from
418 light to dark as development progresses).
419

420 **Comparative transcriptomic analysis of α/β-axon initial growth and γ-axon**
421 **regrowth.**

422 Our bulk smart-seq2 (see materials and methods) dataset includes reads from 8,221
423 distinct genes expressed in at least in one cell type (γ and/or α/β) across six
424 developmental time points. To identify developmentally-regulated patterns of gene
425 expression, we first analyzed the expression profiles of α/β-KCs. We thus concentrated
426 on 3,345 genes that demonstrated dynamic expression in α/β-KCs, i.e., showed
427 statistically significant differential expression during at least one developmental timepoint
428 compared to adult. k-means clustering of those α/β-KC dynamic expression patterns
429 resulted in eight distinct clusters with unique developmental expression profiles (see
430 materials and methods). For example, genes in clusters 1 and 2 are upregulated during
431 the pupal stage but show decreased expression in adults, and thus potentially include
432 activators of axon growth (Figure 2A). In contrast, cluster 5 genes are downregulated
433 during the pupal stage and upregulated in adults, suggesting that they are required for
434 adult-specific functions. Gene Ontology (GO) term analysis further supports this
435 observation. Cluster 1 is enriched for genes involved in axon development and other key
436 developmental processes, including Toll pathway signaling, cytoskeletal rearrangement,
437 and PTEN regulation. In contrast, cluster 5 is enriched for genes associated with synaptic
438 transmission as well as learning and memory (Figure S2).
439 As α/β clusters 1+2 include the best candidates for axon growth promoters but contain a
440 large number of genes (1162 genes; Figure 2A, C), we sought to narrow down the list of
441 candidates. Since we aimed to identify genes required for axon growth in both neuronal
442 types, we decided focus on genes within α/β clusters 1+2 and examine their expression
443 in the γ-KC dataset. We therefore re-clustered the 1,162 genes in α/β clusters 1+2 based
444 on their transcriptional expression in γ-KCs (Figure 2B): cluster 1 was subdivided into

clusters 1A-1J, while cluster 2 was subvidided into 2A-2G. To identify shared genes required for both the initial growth of α/β-axons and the regrowth of γ-axons (Figure 2B–C), we focused on the first three sub-clusters in each heatmap (clusters 1A-C; 2A-C), as they are comprised of genes that are upregulated during axon growth of both neuronal types. From these six clusters, we compiled a set of 676 genes, out of which we selected a subset of 300 genes, which are strongly upregulated during axon growth, associated with biologically relevant functions based on GO term analysis, and have availabe tools to perturb their function (namely – flies expressing RNAi targeting these specific genes). Genes primarily associated with processes less directly related to axon growth—such as cell cycle regulation, DNA replication, chromosome organization, chromatin remodeling, and ribosomal structure—were excluded from further analysis.

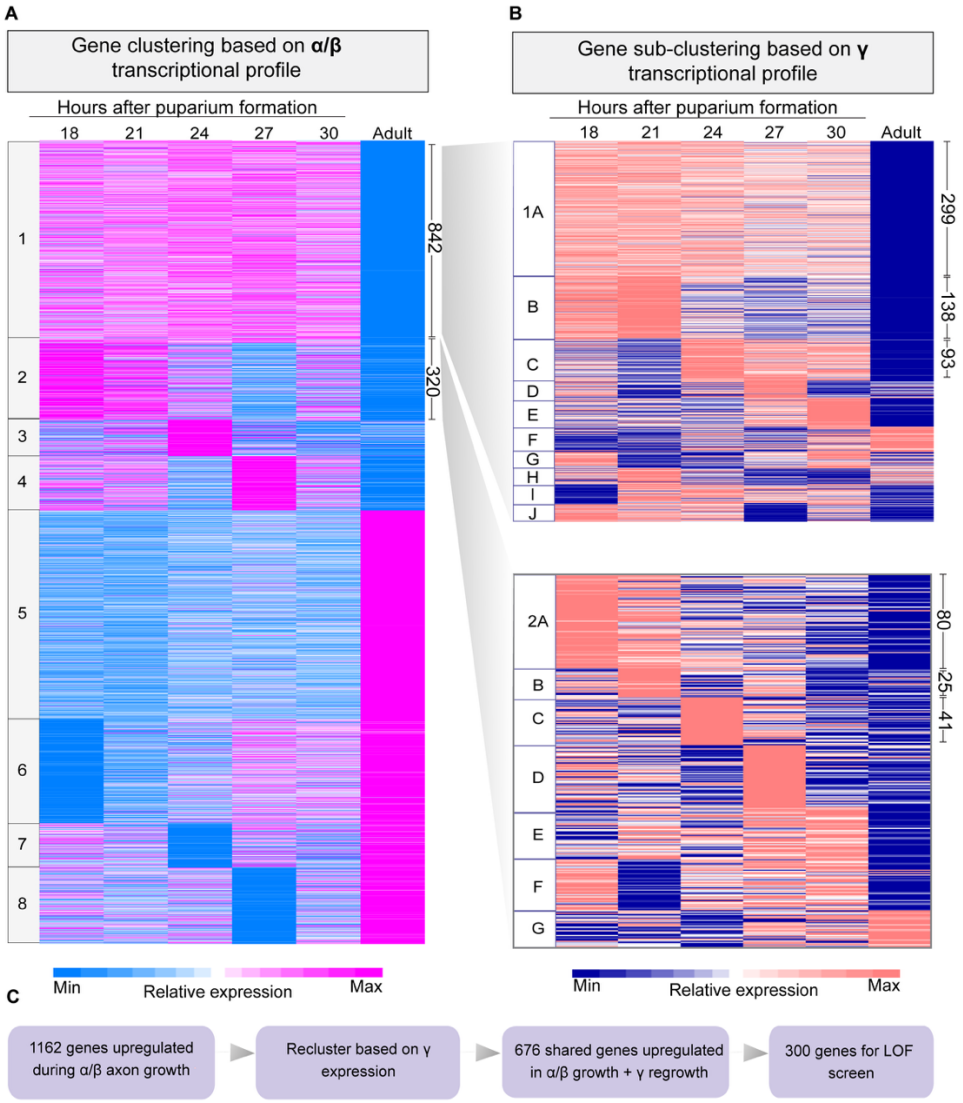

Figure 2. Comparative transcriptomic analysis of α/β-axon initial growth and γ-axon regrowth. (A) Heatmap showing k-means clustering of 3345 differentially expressed genes during α/β-KC development. Light blue and magenta represent low and high relative expression, respectively.
(B) Heatmaps showing k-means re-clustering of 842 genes from cluster 1 or 320 genes from cluster 2 based on their γ-KC transcriptional profiling. Blue and coral represent low and high relative expression, respectively.
For all the heatmaps, each horizontal line describes the relative expression of a single gene. Gene expression was determined in five timepoints after pupa formation (18, 21, 24, 27 and 30 hours APF) and in adult. The number of genes within selected clusters are specified to the right.
(C) A flow chart detailing the criteria used to select candidate genes for the loss-of-function (LOF) screen.

RNAi-based screen identifies 12 genes that are essential for γ- and/or α/β-axon morphology

For the loss-of-function screen, we employed an RNAi-mediated knockdown (KD) strategy, where we expressed RNAi species targeting candidate genes using the OK107-Gal4 driver (which is strongly expressed in all KC types - γ, α'/β' and α/β). γ-axons were visualized in adult brains using a second, independent binary system, via expression of myristylated tandem Tomato (mtdT) driven by R71G10-QF2 – which consistently labels γ-KCs and stochastically labels α/β-KCs. Due to this stochasticity, we additionally stained the brains with anti-Fasciclin II (FasII) antibody, which strongly labels α/β-axons (and weakly labels γ-axons, but never α'/β'-axons).

Out of the 300 genes we screened, KD of 40 genes resulted in various morphological and structural defects (such as thinner axonal lobes, axon misguidance, and branching abnormalities; list of genes in Supplementary Table 2; phenotypic data not shown), 12 of which showed axonal defects – which we categorized into three phenotypic groups (Figure 3): defects in γ-axons but normal α/β-axons (Figure 3C-F); defects in both α/β- and γ-axons (Figure 3G-O); and normal γ-axons but no visible α/β axons (Figure 3P-Q). In addition to the axonal phenotypes that are categorized in Figure 3, KD of several of these 12 genes also resulted in additional morphological defects, such as altered number and shape of cell bodies (data not shown). Notably, 7 of the 12 genes identified in the screen are involved in protein maturation, encompassing post-translational modifications such as folding, cleavage, and prenylation.

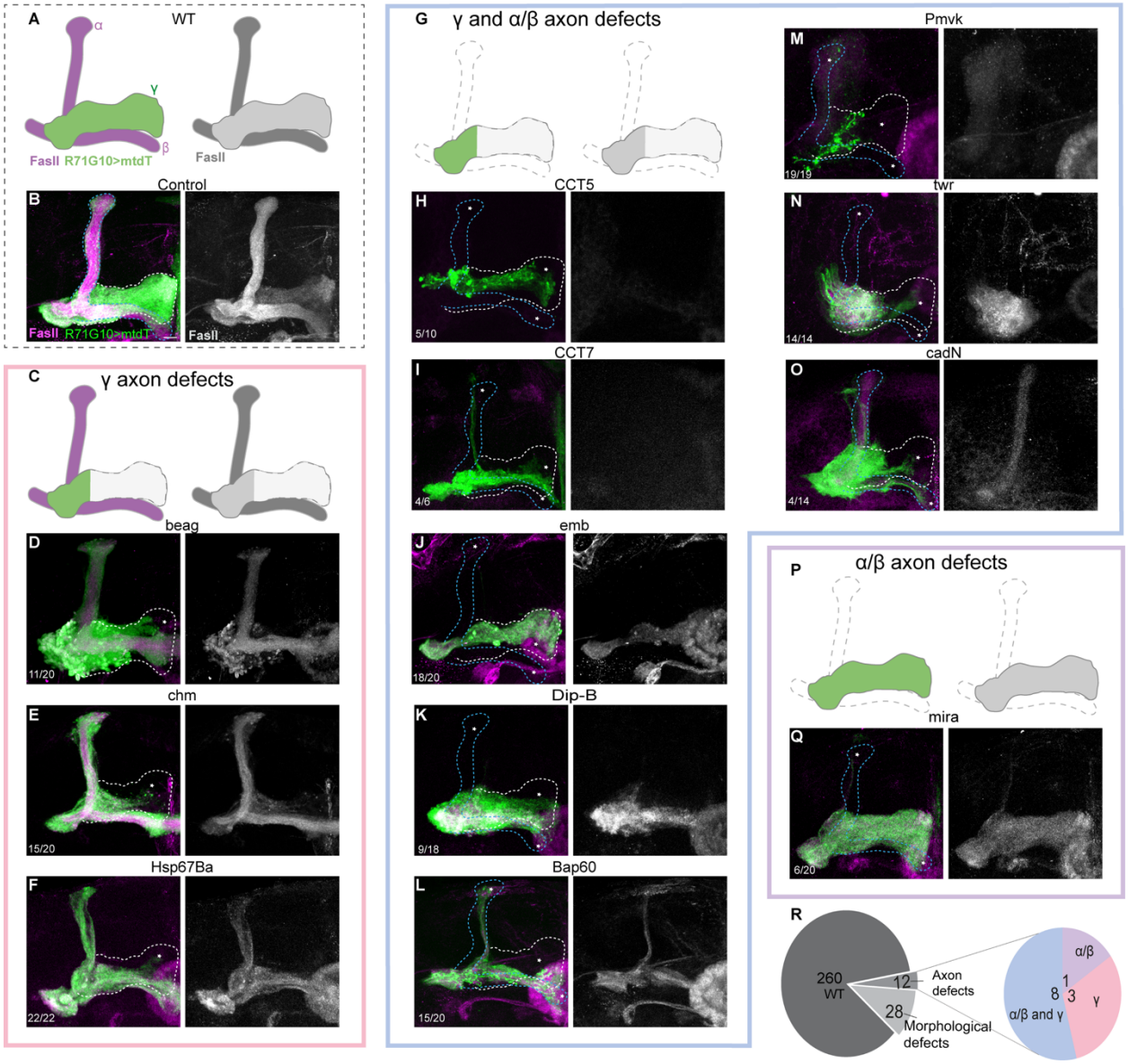

Figure 3. RNAi-based screen identifies 12 genes that are essential for γ- and/or α/β-axon morphology. (A) Schematic of the WT α/β- and γ-axonal lobes, illustrating labeling patterns that match the corresponding confocal images. γ-axons are labeled in green using mtdT:3xHA under the control of R71G10-QF2. FasII is visualized with antibody staining shown in magenta, and also presented separately in greyscale.

(B) Confocal Z-projection of a control MB in which γ-KCs are labeled by mtdT:3xHA (green) driven by R71G10-QF2, and OK107-Gal4 drives the expression of Luciferase. Magenta (left panel) or greyscale (right panel) is anti-FasII staining, which strongly labels α/β-axons and weakly labels γ-axons.

(C,G,P) Schematics of α/β- and/or γ-axon lobe defects.

(D-F,H-O,Q) Confocal Z-projections of adult MBs in which γ-KCs are labeled by mtdT:3xHA (green) driven by R71G10-QF2, with OK107-Gal4 driving expression of RNAi

505 targeting beag (beag; D); chameau (chm; E); Heat shock gene 67Ba (Hsp67Ba; F);
506 Chaperonin containing TCP1 subunit 5 (CCT5; H); Chaperonin containing TCP1 subunit
507 7 (CCT7; I); embargoed (emb; J); Dipeptidase B (Dip-B; K); Brahma associated protein
508 60kD (Bap60; L); Phosphomevalonate kinase (Pmvk; M); twisted bristles roughened eye
509 (twr; N); Cadherin-N (cadN; O); miranda (mira; Q).
510 (R) Pie charts showing the phenotypic distribution of the 300 screened genes (left), and
511 of the axon growth phenotypes of the 12 'positive hits' (right).
512 The putative WT γ- and α/β-lobes are outlined in white and blue, respectively. Asterisks
513 mark the missing part of α/β or γ lobes. Frame colors in (C-Q) represent the phenotypic
514 group as depicted in (R). Numbers represent the fraction of MBs displaying the presented
515 phenotype. Scale bar is 10 μm.
516

517 **Pmvk, cadN and twr are cell-autonomously required for γ-axon regrowth**

518 To inspect the KD phenotypes at better resolution, as well as gain information regarding
519 cell-autonomous requirement, we silenced the genes specifically within neuroblast (NB)
520 clones using the mosaic analysis with a repressible cell marker (MARCM) technique (Lee
521 and Luo, 1999). We used the pan-KC driver OK107-Gal4, resulting in NB clones in which
522 all KC types are labeled as well as express the relevant RNAi. To our surprise, we
523 observed that only Pmvk, cadN and twr showed severe defects in γ-axon regrowth (Figure
524 S3E-G), while the others exhibited γ lobes that were either WT-like, or showed weak
525 regrowth defects (Figure S3). For mira KD, which we expected to affect α/β growth, the
526 lobes seemed to form normally (Figure S3M). In the case of emb, CCT5, and CCT7, the
527 neuroblast clones included only γ-, but no α/β- or α'/β'-KCs (Figure S3B-D), most likely
528 due to a proliferation defect of the neuroblast, which prevented it from generating later
529 born neurons.
530 The proliferation defects in the emb, CCT5 and CCT7 NB clones might suggest that the
531 lack of α/β axons upon KD in the entire population of neurons (Figure 3) is because the
532 neurons were never born, rather than a *bona fida* axon growth defect. To more specifically
533 examine the role of these three candidate genes in α/β-axon growth, we selectively
534 silenced emb, CCT5 and CCT7 in α/β-KCs by inducing MARCM clones at 0h APF (Figure
535 S4) - a time in which α/β-KCs are born (Lee and Luo, 1999). Only single cell clones were
536 visible, suggesting cell-lethality or severe proliferation defects. Importantly, all α/β single-
537 cell clones exhibited WT-like axonal growth (Figure S4), indeed suggesting that the
538 axonal defects observed in Figure 3 are due to non-cell-autonomous effects.

539 Taken together, our findings indicate that Pmvk, cadN, and twr are cell-autonomously
540 required for γ-axon regrowth. For the purpose of this study, we chose to focus on Pmvk,
541 although cadN and twr remain compelling candidates for future investigation.

542 **Pmvk is cell autonomously required for γ-axon regrowth but not for initial axon**
543 **extension of γ- nor α/β-KCs**

544 To further investigate the role of Pmvk in axon growth during development, we specifcially
545 silenced it in γ-KCs using the γ-specific driver R71G10-Gal4. We found that while γ-axons
546 extended normally during the larval stage (L3; Figure 4A-B), the medial γ-lobe failed to
547 fully regrow as evident in the adult stage (Figure 4C-D). To determine whether Pmvk is
548 also required for α/β-axon growth, we silenced it using the R44E04-Gal4 driver (of note,
549 R44E04-Gal4 is strongly expressed in α/β throughout development but also transienty in
550 non-MB neurons, which is why it was not chosen for the RNA profiling experiment;
551 Supplementary Table 1). In contrast to the γ-axons, α/β-axons showed no detectable
552 defects following Pmvk KD (Figure 4E-F).

553 We next used CRISPR/Cas9 to generate a novel Pmvk mutant allele - $Pmvk^{E20}$ - which
554 carries a single-nucleotide substitution resulting in a premature stop codon at amino acid
555 20 (Figure 4M). Due to its homozygous lethality, we analyzed this mutant allele in MARCM
556 clones. In $Pmvk^{E20}$ single-cell γ clones, initial axon growth appeared normal (Figure 4G-
557 H), but, as expected, axons failed to regrow following pruning (Figure 4I-J). In contrast to
558 γ-axons, and in accordance with the RNAi KD results, α/β neuroblast $Pmvk^{E20}$ clones
559 displayed normal axon elongation (Figure 4K-L). Notably, Pmvk mutants produced no NB
560 clones, suggesting an additional requirement for Pmvk in neuroblast proliferation or cell
561 survival.
562

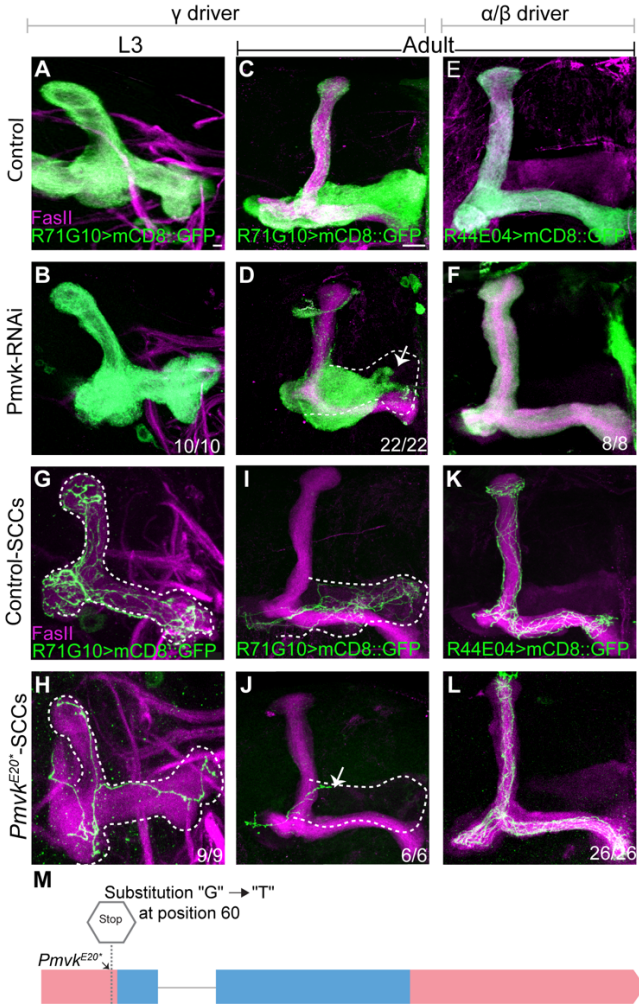

Figure 4. Pmvk is cell autonomously required for γ-axon regrowth but not for initial axon extension of γ nor α/β. (A-F) Confocal Z-projections of L3 (A-B) or adult (C-F) MBs with γ-KCs labeled by mCD8::GFP (green) driven by the γ-specific R71G10-Gal4 (A-D), or the α/β-specific R44E04-Gal4 (E-F). MBs in images (B-F) also express RNAi targeting Pmvk driven by R71G10-Gal4 (B,D) or R44E04-Gal4 (F).

(G-L) Confocal z-projections of control (G,I,K) or *Pmvk*^{E20*} (H,J,L) MARCM clones in L3 (G-H) or Adult (I-L). R71G10-Gal4 (G-J) or R44E04-Gal4 (K-L) drive expression of mCD8::GFP (green). Clones were generated by heat-shocking at 24 hours after egg-laying (G-J) or at 0h APF (K-L).

The full extent of the γ lobe in adult and L3 is outlined in white (as determined by the FasII staining; magenta). Arrows demarcate axon growth defects. Scale bar is 10 μm. Numbers represent the fraction of MBs displaying the presented phenotype.

(M) Schematic representation of the *Pmvk*^{E20*} mutant allele, which includes a single-nucleotide substitution (G>T) at position 60, corresponding to amino acid 20, leading to the replacement of glutamic acid (E) with a stop codon.

The mevalonate pathway is essential for γ-axon regrowth

Pmvk is part of the mevalonate pathway – a highly conserved metabolic enzymatic pathway that consumes acetyl coenzyme A to synthesize a wide variety of isoprenoids, such as cholesterol, dolichol, and ubiquinone (Figure 5D; Edwards and Ericsson, 2025; Hinson et al., 1997). We knocked down the additional seven key enzymes in the pathway and found that pan-KC silencing of either Hmgcr or Mvk led to seemingly similar γ-regrowth defects (but not defects in α/β extension; Figure 5A-C), suggesting an overall requirement of the mevalonate pathway for γ-axon regrowth.

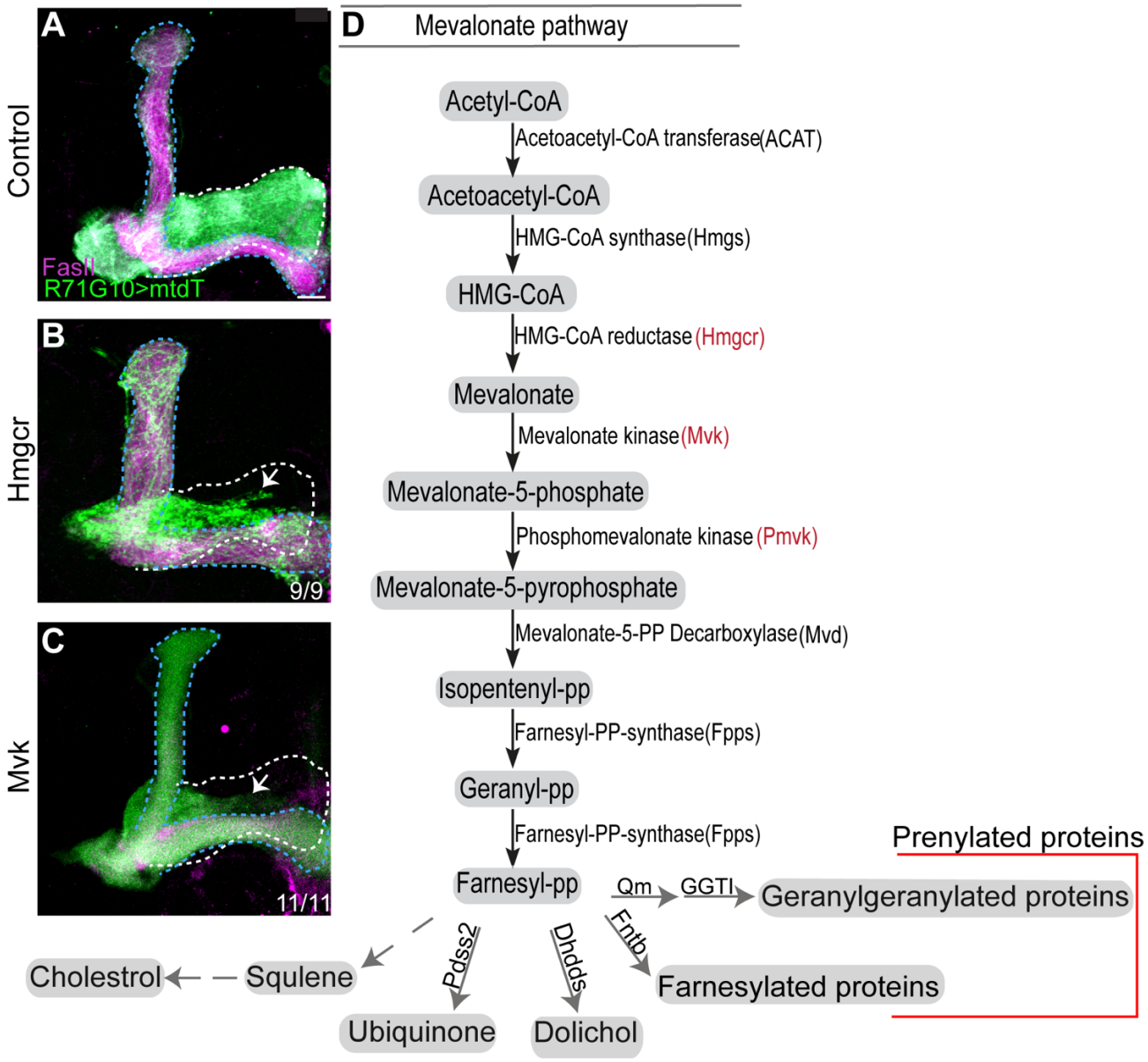

590 **Figure 5. The mevalonate pathway is essential for γ-axon regrowth**. (A-C) Confocal
591 Z-projections of adult MBs from control (A) or those expressing RNAi targeting Hmgcr (B)
592 or Mvk (C) driven by the pan-KC driver OK107-Gal4. γ-KCs are labeled by mtdT:3xHA
593 (green) driven by R71G10-QF2. Magenta is FasII staining. The putative WT α/β- and
594 putative γ-lobes are outlined in blue and white, respectively. Arrows indicate axon growth
595 defects. Numbers represent the fraction of MBs displaying the presented phenotype.
596 Scale bar is 10 μm.
597 (D) A schematic of the mevalonate pathway, illustrating key metabolites and enzymes.
598 Enzymes shown in red are those found to influence γ-axon development. The diagram
599 also highlights the different downstream routes that FPP can take—either toward the
600 synthesis of sterol isoprenoids (e.g., cholesterol) or non-sterol isoprenoids (such as
601 ubiquinone, dolichol, and isopentenyl-tRNA). Additionally, FPP serves as a precursor for
602 protein prenylation, which occurs in two main forms: farnesylation and
603 geranylgeranylation. The dashed arrows emphasize that cholesterol biosynthesis is
604 absent in *Drosophila*.
605

606 **Pmvk likely regulates axon regrowth via the TOR pathway**

607 The mevalonate pathway generates a common isoprenoid product that can be directed
608 into five major downstream pathways (Figure 5D). In mammals, one of these is
609 cholesterol biosynthesis, which is absent in *Drosophila*; instead, flies must obtain
610 cholesterol from their diet (Cesur et al., 2023). The other four branches are: (2) ubiquinone
611 synthesis, (3) dolichol synthesis, and (4–5) protein prenylation, through the addition of
612 either farnesyl (4) or geranylgeranyl (5) groups. Prenylation increases protein
613 hydrophobicity, thereby regulating their association with cellular membranes and
614 influencing their function.
615 To test which of these branches might contribute to axon regrowth, we knocked down the
616 major enzymes required for each process. However, none of these manipulations
617 produced a regrowth defect (Figure S5). This could be due to insufficient efficiency of
618 RNAi KD, or because simultaneous KD of two or more enzymes is necessary to reveal
619 an effect. Since we were unable to pinpoint a specific downstream pathway, we decided
620 to focus on the prenylation branch, as it was previously shown that prenylated proteins,
621 such as the Rho GTPase and Rheb (Ras homolog enriched in brain), are associated with
622 axon growth (Ng and Luo, 2004; Hall and Lalli, 2010).
623 Importantly, previous work from our lab demonstrated that the nuclear receptor unfulfilled
624 (UNF) promotes axon regrowth by activating a program mediated, at least in part, by the

625 Rheb-TOR-S6 kinase pathway (Figure 6A; Yaniv et al., 2012). We thus conducted rescue
626 experiments in Pmvk mutants by overexpressing Rho, Rheb, and most importantly - a
627 constitutively active variant of the Rheb downstream effector S6 kinase ($S6K^{CA}$).
628 Overexpression of Rho within Pmvk mutant clones showed no suppressive effect on the
629 regrowth defect (Fig. 6B,E). Rheb overexpression did not significantly rescue γ-axon
630 regrowth in the Pmvk mutant background (3/7 clones; Fig. 6B,F), which is consistent with
631 the requirement for prenylation to achieve full Rheb activity and TOR activation. In
632 contrast, $S6K^{CA}$ overexpression showed an obvious trend toward suppression of the
633 regrowth defect (7/10 clones displaying near-complete γ-axon extension; Fig. 6B,G).
634 However, this effect did not reach statistical significance with the current sample size,
635 which we unfortunately were unable to further increase (see acknowledgements). Taken
636 together, these results suggest that Pmvk promotes γ-axon regrowth, at least in part,
637 through the Rheb–TOR pathway.

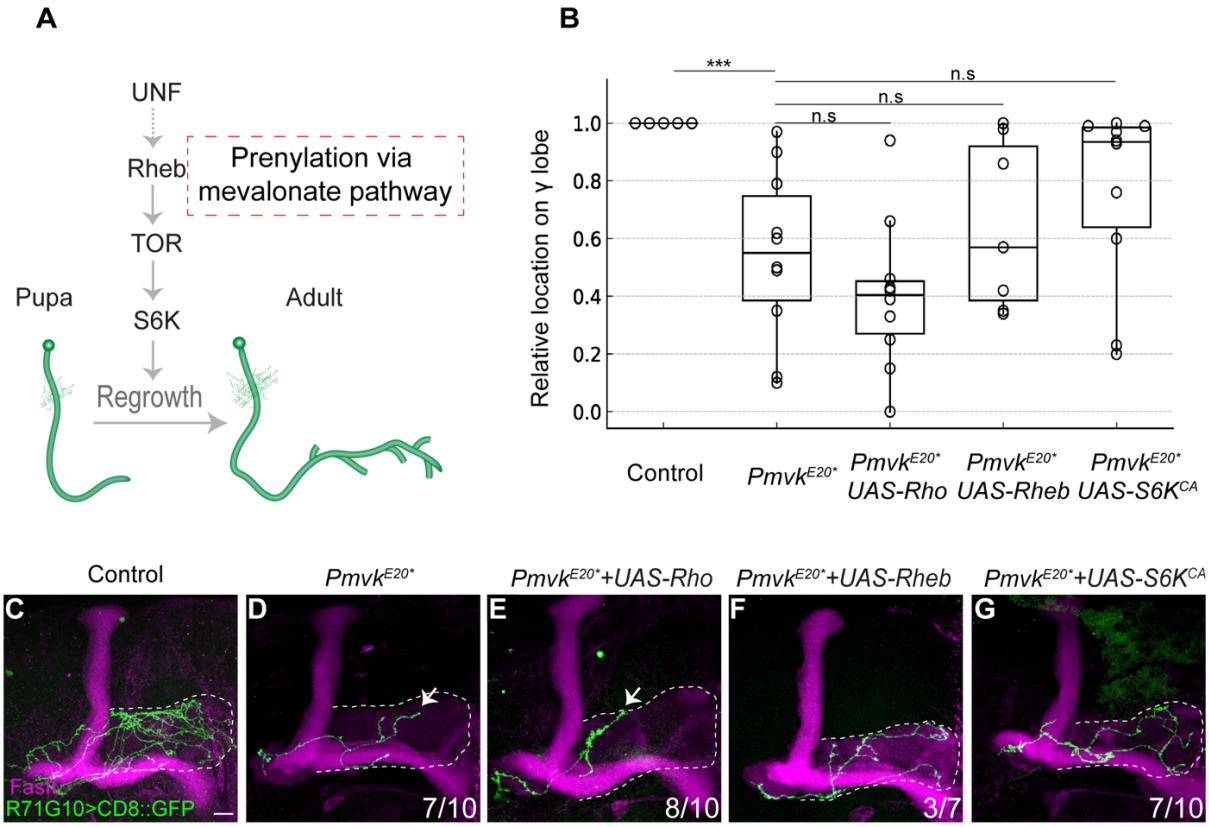

638

639 **Figure 6. Pmvk likely regulates axon regrowth via the TOR pathway**. (A) Scheme of
640 developing γ-KCs in which UNF promotes regrowth via the TOR pathway (adapted from

641 Yaniv et al., 2012). Rheb is a CAAX protein that undergoes prenylation, enabling its
642 translocation to the plasma membrane to activate downstream effectors.
643 (B) Quantification of axon regrowth for the genotypes displayed in (C-G). The x/y ratio
644 indicates relative axon position along the adult γ lobe (quantification described in Figure
645 S7). Box plots represent the median (line), interquartile range (box), and spread within
646 1.5×IQR (whiskers), circles indicate individual data points. Groups were compared using
647 one-way ANOVA on logit-transformed data followed by Dunnett's post-hoc test. A
648 significant difference was observed only between control and *Pmvk*^{E20*} (***$p < 0.001$).
649 Comparisons of *Pmvk*^{E20*} only with *Pmvk*^{E20*} and UAS-Rho ($p = 0.696$), or UAS-Rheb (p
650 $= 0.704$), or *UAS-S6K*^{CA} ($p = 0.120$) were not significant.
651 (C-G) Confocal Z-projections of γ single-cell MARCM clones in adult MBs, either control
652 (C, comprised of multiple single cell clones), *Pmvk*^{E20*} homozygous mutant (D), or
653 *Pmvk*^{E20*} homozygous mutant also overexpressing Rho (E), Rheb (F) or *S6K*^{CA} (G).
654 The γ-specific driver R71G10-Gal4 drives expression of membranal GFP (mCD8::GFP;
655 green). Magenta is FasII staining. The γ lobe is outlined by a dashed white line. Arrows
656 indicate axon growth defects. Numbers represent the fraction of MBs displaying the
657 presented phenotype. Scale bar is 10 μm.
658

659 **Discussion**

660 How axon growth is regulated across different cellular and developmental contexts
661 remains largely unknown. In this study, we used the remodeling MB as a model to uncover
662 the transcriptional profiles of two lineage-related neuron types - γ- and α/β-KCs - which
663 undergo developmental axon regrowth and initial axon growth, respectively, in similar
664 spatiotemporal conditions. By comparing their transcriptional programs, we identified
665 shared and unique expression patterns, highlighting candidates for an RNAi screen
666 through which we identified genes promoting γ- and/or α/β-axon formation. One gene we
667 found to be essential for regrowth of γ-axons is Pmvk, an enzyme in the mevalonate
668 pathway responsible for isoprenoid biosynthesis. While Pmvk has not previously been
669 directly linked to axon growth, isoprenoids are known to be required for the prenylation of
670 small GTPases such as RhoA, Ras, and Cdc42—key regulators of the cytoskeleton and
671 axon guidance (Hakeda-Suzuki et al., 2002; Hall and Lalli, 2010; Lee et al., 2021; Ng and
672 Luo, 2004). Our findings suggest that Pmvk contributes to axon regrowth, at least in part,
673 by supporting the membrane localization of Rheb, a prenylation-dependent GTPase
674 previously shown to promote γ-axon regrowth (Yaniv et al., 2012).
675 A major strength of this study lies in its high temporal resolution, enabled by RNA-seq
676 analysis across five developmental stages (at 3-hour intervals) plus adulthood. This was

677 enabled due to a Gal4 line that we characterized and found to be specific to α/β-KCs
678 throughout development, which allowed us to capture these neurons during active axon
679 growth. Notably, our screening approach was aimed at uncovering shared genes required
680 for both α/β growth and γ regrowth. However, despite identifying several γ regrowth-
681 promoting genes, we did not uncover any strong candidates cell-autonomously required
682 for α/β axon growth. This may reflect the robustness and/or redundancy of the genetic
683 programs controlling α/β axon extension, where the loss of individual genes might be
684 buffered by compensatory pathways. Previous studies suggested that larval γ axons
685 provide a structural template for later-born KC types, including α/β-KCs, which follow a
686 relatively stereotyped and stable developmental trajectory (Kurusu et al., 2002). Most of
687 the genes known to affect α/β-KC development, such as FasII, Drl, and Netrin, impact
688 guidance, branching, or stability but not necessarily initial axon extension (Bates et al.,
689 2014; Fushima and Tsujimura, 2007; Hatch et al., 2021; Kang et al., 2019; Lin et al., 2009;
690 Reynaud et al., 2015). One exception is twinstar (tsr), which encodes Cofilin and is
691 required for early α/β axon growth, highlighting actin regulation as a potential neuron-
692 intrinsic vulnerability in these cells (Ng and Luo, 2004). Similarly, Sickie was shown to be
693 required for early α/β growth, functioning through a non-canonical Rac–Cofilin pathway
694 (Abe et al., 2014). Notably, even in these cases, a scenario of normal initial growth
695 followed by late developmental axonal degeneration has not been directly ruled out. Our
696 findings suggest that combinatorial loss-of-function experiments, or temporally-targeted
697 approaches, may be necessary to uncover additional regulators of α/β initial growth.
698 Our data provide a valuable resource for the *Drosophila* neuroscience community,
699 particularly given that γ- and α/β-KCs together constitute the majority of the intrinsic MB
700 neurons. The identification of Pmvk as a growth-promoting factor opens new avenues for
701 dissecting how metabolic processes shape axonal remodeling. Since Pmvk is involved in
702 isoprenoid synthesis required for protein prenylation, its role likely intersects with the
703 activity of small GTPases such as Rheb, which are essential for growth signaling. This
704 suggests a model in which metabolic enzymes like Pmvk act upstream to facilitate the
705 activation of growth-promoting pathways through post-translational modification of key
706 signaling molecules. Understanding this link between metabolism and signaling may shed

707 light on how neurons integrate internal metabolic states with external developmental cues
708 to regulate growth.
709 The broader role of the mevalonate pathway in axon growth is complex and context-
710 dependent. While some studies have shown that inhibiting this pathway impairs axon
711 extension, others suggest it may promote regeneration under certain conditions (Li et al.,
712 2016; Schulz et al., 2004). This may reflect the dual role of the pathway in both isoprenoid
713 and cholesterol synthesis. Pharmacological inhibition of the pathway aimed at reducing
714 cholesterol levels —as with the widely used statins, which directly inhibit Hmgcr, the rate-
715 limiting enzyme of the mevalonate pathway—could thus potentially have unintended
716 effects on neuronal growth. Moreover, this pathway is tightly regulated by nutrient-
717 sensitive signals, including insulin and TOR signaling (Belgacem and Martin, 2007), which
718 activate SREBP, a transcription factor controlling lipid metabolism regulators like Hmgcr.
719 In *Drosophila*, SREBP is known to regulate lipid homeostasis; therefore, it would be
720 interesting to examine whether SREBP is required for neuronal remodeling (Seegmiller
721 et al., 2002). Together, our findings highlight a critical link between cellular metabolism,
722 signaling, and axon growth, suggesting that a neuron's ability to remodel relies on
723 sustained metabolic support and coordination between growth and nutrient-sensing
724 pathways.
725 Finally, understanding axon growth capacity is key for understanding what limits axon
726 regeneration following injury. Our transcriptomic and genetic analyses identify candidate
727 genes that may therefore be relevant to axon repair following injury. Future efforts to injure
728 γ-axons and compare their injury-evoked transcriptional program with those of initial α/β
729 growth and developmental γ regrowth could provide valuable insights into shared and
730 regeneration-specific molecular pathways.
731

732 **Acknowledgements**

733 We thank the Bloomington Drosophila Stock Center and the Vienna Drosophila Resource
734 Center for providing fly stocks. Monoclonal antibodies were obtained from the
735 Developmental Studies Hybridoma Bank, created under the auspices of the NICHD and
736 maintained by the University of Iowa. We are grateful to D. Robbins and to the staff of the
737 Crown Institute for Genomics, INCPM for performing the RNA-seq, and to E. Hagai for

assistance with cell sorting. This work was supported by the Minerva Foundation (grant # 714145) with funding from the Federal German Ministry of Education and Research, the Samowitz Foundation Trust, the Estate of Gerald Alexander, and by the European Research Council (ERC) Advanced Grant #101054886, “NeuRemodelBehavior”. O.S. is the incumbent of the Prof. Erwin Netter Professorial Chair of Cell Biology.

On June 15, 2025, our laboratory was directly hit by an Iranian missile and was completely destroyed, which unfortunately currently limits our ability to increase sample size (Figure 6) and to provide the Pmvk mutant allele generated in this study (which we are now in the process of rebuilding).

References

Abe, T., Yamazaki, D., Murakami, S., Hiroi, M., Nitta, Y., Maeyama, Y., Tabata, T., 2014. The NAV2 homolog Sickie regulates F-actin-mediated axonal growth in Drosophila mushroom body neurons via the non-canonical Rac-Cofilin pathway. Development 141, 4716–4728. https://doi.org/10.1242/dev.113308

Alyagor, I., Berkun, V., Keren-Shaul, H., Marmor-Kollet, N., David, E., Mayseless, O., Issman-Zecharya, N., Amit, I., Schuldiner, O., 2018. Combining Developmental and Perturbation-Seq Uncovers Transcriptional Modules Orchestrating Neuronal Remodeling. Developmental Cell 47, 38-52.e6. https://doi.org/10.1016/j.devcel.2018.09.013

Bates, K.E., Sung, C., Hilson, L., Robinow, S., 2014. unfulfilled Interacting Genes Display Branch-Specific Roles in the Development of Mushroom Body Axons in Drosophila melanogaster. G3 Genes|Genomes|Genetics 4, 693–706. https://doi.org/10.1534/g3.113.009829

Belgacem, Y.H., Martin, J.-R., 2007. Hmgcr in the Corpus Allatum Controls Sexual Dimorphism of Locomotor Activity and Body Size via the Insulin Pathway in Drosophila. PLOS ONE 2, 1–11. https://doi.org/10.1371/journal.pone.0000187

Belle, J.S.D., Heisenberg, M., 1994. Associative odor learning in Drosophila abolished by chemical ablation of mushroom bodies. Science. https://doi.org/10.1126/science.8303280

Bornstein, B., Meltzer, H., Adler, R., Alyagor, I., Berkun, V., Cummings, G., Reh, F., Keren-Shaul, H., David, E., Riemensperger, T., Schuldiner, O., 2021. Transneuronal Dpr12/DIP-δ interactions facilitate compartmentalized dopaminergic innervation of Drosophila mushroom body axons. The EMBO Journal 40, e105763. https://doi.org/10.15252/embj.2020105763

Bornstein, B., Zahavi, E.E., Gelley, S., Zoosman, M., Yaniv, S.P., Fuchs, O., Porat, Z., Perlson, E., Schuldiner, O., 2015. Developmental Axon Pruning Requires Destabilization of Cell Adhesion by JNK Signaling. Neuron 88, 926–940. https://doi.org/10.1016/j.neuron.2015.10.023

Bradke, F., 2022. Mechanisms of Axon Growth and Regeneration: Moving between Development and Disease. J. Neurosci. 42, 8393. https://doi.org/10.1523/JNEUROSCI.1131-22.2022

780 Cesur, M.F., Basile, A., Patil, K.R., Çakır, T., 2023. A new metabolic model of Drosophila
781 melanogaster and the integrative analysis of Parkinson's disease. Life Sci. Alliance
782 6, e202201695. https://doi.org/10.26508/lsa.202201695
783 Dobin, A., Davis, C.A., Schlesinger, F., Drenkow, J., Zaleski, C., Jha, S., Batut, P., Chaisson,
784 M., Gingeras, T.R., 2013. STAR: ultrafast universal RNA-seq aligner. Bioinformatics 29,
785 15–21. https://doi.org/10.1093/bioinformatics/bts635
786 Edwards, P.A., Ericsson, J., 2025. STEROLS AND ISOPRENOIDS: SIGNALING
787 MOLECULES DERIVED FROM THE CHOLESTEROL BIOSYNTHETIC
788 PATHWAY.
789 Fushima, K., Tsujimura, H., 2007. Precise control of fasciclin II expression is required for adult
790 mushroom body development in Drosophila. Development, Growth & Differentiation 49,
791 215–227. https://doi.org/10.1111/j.1440-169X.2007.00922.x
792 Hakeda-Suzuki, S., Ng, J., Tzu, J., Dietzl, G., Sun, Y., Harms, M., Nardine, T., Luo, L., Dickson,
793 B.J., 2002. Rac function and regulation during Drosophila development. Nature 416,
794 438–442. https://doi.org/10.1038/416438a
795 Hall, A., Lalli, G., 2010. Rho and Ras GTPases in Axon Growth, Guidance, and Branching. Cold
796 Spring Harbor Perspectives in Biology 2, a001818–a001818.
797 https://doi.org/10.1101/cshperspect.a001818
798 Hatch, H.A., Belalcazar, H.M., Marshall, O.J., Secombe, J., 2021. A KDM5–Prospero
799 transcriptional axis functions during early neurodevelopment to regulate mushroom body
800 formation. eLife 10, e63886. https://doi.org/10.7554/eLife.63886
801 Hilton, B.J., Husch, A., Schaffran, B., Lin, T., Burnside, E.R., Dupraz, S., Schelski, M., Kim, J.,
802 Müller, J.A., Schoch, S., Imig, C., Brose, N., Bradke, F., 2022. An active vesicle priming
803 machinery suppresses axon regeneration upon adult CNS injury. Neuron 110, 51-69.e7.
804 https://doi.org/10.1016/j.neuron.2021.10.007
805 Hinson, D.D., Chambliss, K.L., Toth, M.J., Tanaka, R.D., Gibson, K.M., 1997. Post-translational
806 regulation of mevalonate kinase by intermediates of the cholesterol and nonsterol
807 isoprene biosynthetic pathways. Journal of Lipid Research 38, 2216–2223.
808 https://doi.org/10.1016/S0022-2275(20)34935-X
809 Kang, H., Zhao, J., Jiang, X., Li, G., Huang, W., Cheng, H., Duan, R., 2019. Drosophila Netrin-
810 B controls mushroom body axon extension and regulates courtship-associated learning
811 and memory of a Drosophila fragile X syndrome model. Molecular Brain 12, 52.
812 https://doi.org/10.1186/s13041-019-0472-1
813 Kurusu, M., Awasaki, T., Masuda-Nakagawa, L.M., Kawauchi, H., Ito, K., Furukubo-Tokunaga,
814 K., 2002. Embryonic and larval development of the Drosophila mushroom bodies:
815 concentric layer subdivisions and the role of fasciclin II. Development 129, 409–419.
816 https://doi.org/10.1242/dev.129.2.409
817 Lee, S.J., Zdradzinski, M.D., Sahoo, P.K., Kar, A.N., Patel, P., Kawaguchi, R., Aguilar, B.J.,
818 Lantz, K.D., McCain, C.R., Coppola, G., Lu, Q., Twiss, J.L., 2021. Selective axonal
819 translation of the mRNA isoform encoding prenylated Cdc42 supports axon growth.
820 Journal of Cell Science 134, jcs251967. https://doi.org/10.1242/jcs.251967
821 Lee, T., Lee, A., Luo, L., 1999. Development of the Drosophila mushroom bodies: Sequential
822 generation of three distinct types of neurons from a neuroblast. Development 126, 4065–
823 4076.

824 Lee, T., Luo, L., 1999. Mosaic analysis with a repressible neurotechnique cell marker for studies
825 of gene function in neuronal morphogenesis. Neuron. https://doi.org/10.1016/S0896-
826 6273(00)80701-1
827 Lee, T., Marticke, S., Sung, C., Robinow, S., Luo, L., 2000. Cell-autonomous requirement of the
828 USP/EcR-B ecdysone receptor for mushroom body neuronal remodeling in Drosophila.
829 Neuron 28, 807–818. https://doi.org/10.1016/S0896-6273(00)00155-0
830 Li, H., Kuwajima, T., Oakley, D., Nikulina, E., Hou, J., Yang, W.S., Lowry, E.R., Lamas, N.J.,
831 Amoroso, M.W., Croft, G.F., Hosur, R., Wichterle, H., Sebti, S., Filbin, M.T., Stockwell,
832 B., Henderson, C.E., 2016. Protein Prenylation Constitutes an Endogenous Brake on
833 Axonal Growth. Cell Reports 16, 545–558. https://doi.org/10.1016/j.celrep.2016.06.013
834 Lin, S., Huang, Y., Lee, T., 2009. Nuclear Receptor Unfulfilled Regulates Axonal Guidance and
835 Cell Identity of Drosophila Mushroom Body Neurons. PLOS ONE 4, 1–12.
836 https://doi.org/10.1371/journal.pone.0008392
837 Lindner, J., Dassa, B., Wigoda, N., Stelzer, G., Feldmesser, E., Prilusky, J., Leshkowitz, D.,
838 2025. UTAP2: an enhanced user-friendly transcriptome and epigenome analysis pipeline.
839 BMC Bioinformatics 26, 79. https://doi.org/10.1186/s12859-025-06090-8
840 Love, M.I., Huber, W., Anders, S., 2014. Moderated estimation of fold change and dispersion for
841 RNA-seq data with DESeq2. Genome Biology 15, 550. https://doi.org/10.1186/s13059-
842 014-0550-8
843 Marmor-Kollet, N., Schuldiner, O., 2016. Contrasting developmental axon regrowth and neurite
844 sprouting of Drosophila mushroom body neurons reveals shared and unique molecular
845 mechanisms. Developmental Neurobiology 76, 262–276.
846 https://doi.org/10.1002/dneu.22312
847 Ng, J., Luo, L., 2004. Rho GTPases Regulate Axon Growth through Convergent and Divergent
848 Signaling Pathways. Neuron 44, 779–793. https://doi.org/10.1016/j.neuron.2004.11.014
849 Picelli, S., Faridani, O.R., Björklund, Å.K., Winberg, G., Sagasser, S., Sandberg, R., 2014. Full-
850 length RNA-seq from single cells using Smart-seq2. Nature Protocols 9, 171–181.
851 https://doi.org/10.1038/nprot.2014.006
852 Rabinovich, D., Yaniv, S.P., Alyagor, I., Schuldiner, O., 2016. Nitric Oxide as a Switching
853 Mechanism between Axon Degeneration and Regrowth during Developmental
854 Remodeling. Cell 164, 170–182. https://doi.org/10.1016/j.cell.2015.11.047
855 Reynaud, E., Lahaye, L.L., Boulanger, A., Petrova, I.M., Marquilly, C., Flandre, A., Martianez,
856 T., Privat, M., Noordermeer, J.N., Fradkin, L.G., Dura, J.-M., 2015. Guidance of
857 Drosophila Mushroom Body Axons Depends upon DRL-Wnt Receptor Cleavage in the
858 Brain Dorsomedial Lineage Precursors. Cell Reports 11, 1293–1304.
859 https://doi.org/10.1016/j.celrep.2015.04.035
860 Rozo, J.A., Martínez-Gallego, I., Rodríguez-Moreno, A., 2024. Cajal, the neuronal theory and
861 the idea of brain plasticity. Frontiers in Neuroanatomy 18.
862 https://doi.org/10.3389/fnana.2024.1331666
863 Schuldiner, O., Yaron, A., 2015. Mechanisms of developmental neurite pruning. Cellular and
864 Molecular Life Sciences 72, 101–119. https://doi.org/10.1007/s00018-014-1729-6
865 Schulz, J.G., Bösel, J., Stoeckel, M., Megow, D., Dirnagl, U., Endres, M., 2004. HMG-CoA
866 reductase inhibition causes neurite loss by interfering with geranylgeranylpyrophosphate
867 synthesis. Journal of Neurochemistry 89, 24–32. https://doi.org/10.1046/j.1471-
868 4159.2003.02305.x

869 Seegmiller, A.C., Dobrosotskaya, I., Goldstein, J.L., Ho, Y.K., Brown, M.S., Rawson, R.B.,
870 2002. The SREBP Pathway in Drosophila: Regulation by Palmitate, Not Sterols.
871 Developmental Cell 2, 229–238. https://doi.org/10.1016/S1534-5807(01)00119-8
872 Sudarsanam, S., Yaniv, S., Meltzer, H., Schuldiner, O., 2020. Cofilin regulates axon growth and
873 branching of Drosophila γ-neurons. Journal of Cell Science 133.
874 https://doi.org/10.1242/jcs.232595
875 Sutherland, T.C., Geoffroy, C.G., 2020. The Influence of Neuron-Extrinsic Factors and Aging on
876 Injury Progression and Axonal Repair in the Central Nervous System. Frontiers in Cell
877 and Developmental Biology Volume 8-2020. https://doi.org/10.3389/fcell.2020.00190
878 Xie, Q., Brbic, M., Horns, F., Kolluru, S.S., Jones, R.C., Li, J., Reddy, A.R., Xie, A., Kohani, S.,
879 Li, Z., McLaughlin, C.N., Li, T., Xu, C., Vacek, D., Luginbuhl, D.J., Leskovec, J.,
880 Quake, S.R., Luo, L., Li, H., 2021. Temporal evolution of single-cell transcriptomes of
881 *Drosophila* olfactory projection neurons. eLife 10, e63450.
882 https://doi.org/10.7554/eLife.63450
883 Yaniv, S.P., Issman-Zecharya, N., Oren-Suissa, M., Podbilewicz, B., Schuldiner, O., 2012. Axon
884 regrowth during development and regeneration following injury share molecular
885 mechanisms. Current Biology 22, 1774–1782. https://doi.org/10.1016/j.cub.2012.07.044
886 Yaniv, S.P., Meltzer, H., Alyagor, I., Schuldiner, O., 2020. Developmental axon regrowth and
887 primary neuron sprouting utilize distinct actin elongation factors. Journal of Cell Biology
888 219. https://doi.org/10.1083/jcb.201903181
889 Zheng, B., Tuszynski, M.H., 2023. Regulation of axonal regeneration after mammalian spinal
890 cord injury. Nature Reviews Molecular Cell Biology 24, 396–413.
891 https://doi.org/10.1038/s41580-022-00562-y
892 Zhou, Y., Zhou, B., Pache, L., Chang, M., Khodabakhshi, A.H., Tanaseichuk, O., Benner, C.,
893 Chanda, S.K., 2019. Metascape provides a biologist-oriented resource for the analysis of
894 systems-level datasets. Nature Communications 10, 1523.
895 https://doi.org/10.1038/s41467-019-09234-6
896
897